

Characterization of cerium-based conversion coatings for corrosion protection of AISI-1010 commercial carbon steel

E. Onofre-Bustamante · M. A. Domínguez-Crespo ·
A. M. Torres-Huerta · A. Olvera-Martínez ·
J. Genescá-Llongueras · F. J. Rodríguez-Gómez

Received: 21 October 2008 / Revised: 21 May 2009 / Accepted: 26 May 2009 / Published online: 23 June 2009
© Springer-Verlag 2009

Abstract The role of hydrogen peroxide in the formation of cerium conversion coatings by immersing AISI 1010 commercial carbon steel substrates into solutions containing various concentrations of CeCl_3 (0.1, 1, and 10 g L^{-1}) has been investigated as an alternative method for their protection against corrosion. The deposits prepared from the solutions with H_2O_2 consist of yellow thin and non-uniform coatings with agglomerates of small CeO_2 and Ce_2O_3 crystallites whose sizes increased over the metallic surface as the cerium concentration was increased. Cerium pre-treatments in the presence of H_2O_2 displayed layers that were rougher than those synthesized without H_2O_2 . A comparison with the chromate conversion pre-treatment is also simultaneously carried out with the discussion of the possible reactions involved in the different stages of process. The coating obtained from the solution containing 0.1 g in 1,000 mL produced better corrosion resistance on the substrate than that observed for its counterparts due to

the fact that the surface was more uniformly covered by the conversion coating. The addition of H_2O_2 to the cerate baths improves visible roughness, corrosion resistance of the conversion coatings and bond strength because hydrogen peroxide acts as an oxygen source during the formation of the coatings.

Keywords Corrosion properties · Chemical conversion coatings · Cerium salts · Hydrogen peroxide

Introduction

Chemical conversion coatings (CCCs) are used in different metal finishings to impart corrosion protection and improve adhesion of paint systems to the underlying metal [1, 2]. However, the adverse impact of CCCs on human health and the environment have brought about a regulatory regime where chromate conversion coatings (CrCCs) are being phased out [3–6]. Rare earth conversion coatings have been reported as one of a number of alternatives [7–9]. In particular cerium conversion coatings (CeCCs) are one of the most promising environmentally friendly surface treatments for a range of metals including aluminum alloys [10–12], magnesium alloys [13, 14], tin [15], and zinc alloys [16, 17].

One important feature of a $\text{CeO}_2\cdot\text{H}_2\text{O}$ layer deposited on an oxidizable metal is its ability to “self-heal” when damage occurs. This interesting behavior has been attributed to the interconversion of Ce^{3+} and $\text{Ce}(\text{OH})_2^{2+}$ ions which is possible in an aqueous solution following the recently updated Pourbaix diagram [18, 19]. Then, the $\text{CeO}_2\cdot\text{H}_2\text{O}$ coating is supposed to act similarly to the classical CCCs; however, the efficiency of the various processes using

Electronic supplementary material The online version of this article (doi:10.1007/s10008-009-0871-9) contains supplementary material, which is available to authorized users.

E. Onofre-Bustamante · A. Olvera-Martínez ·
J. Genescá-Llongueras · F. J. Rodríguez-Gómez (✉)
Edificio D Facultad de Química,
Departamento de Ingeniería Metalúrgica,
Universidad Nacional Autónoma de México,
Ciudad Universitaria,
C.P.04510 México, DF, México
e-mail: fxavier@servidor.unam.mx

M. A. Domínguez-Crespo · A. M. Torres-Huerta
Grupo de Ingeniería en Procesamiento de Materiales CICATA-IPN,
Instituto Politécnico Nacional,
Unidad Altamira. Km 14.5,
Carretera Tampico-Puerto Industrial Altamira,
C. P. 89600 Altamira, Tamaulipas, México

cerium salts, and developed until now, has never really equaled that of the excellent CrCCs. Different approaches to cerium-based conversion coatings have been investigated. The first method involves early work, where the deposition of a conversion coating onto metal surfaces results from immersion for several days in simple cerium salt solutions at near-neutral pH [14–17, 20]. The second type of formulation involves H_2O_2 -assisted solutions, which consist of cerium salt solutions containing hydrogen peroxide (H_2O_2) [2, 10, 12, 13, 17, 20–23] that can result in a deposition at much faster rates, which suggests that H_2O_2 interacts with the cerium species in the solution.

As in the metallurgical industry carbon steel keeps playing an important role in different applications, investigation on its behavior during pre-treatment and its influence on subsequent surface treatments is still important. Chemical conversion coatings for commercial carbon steel based on the immersion in cerium and cerium/hydrogen peroxide solutions can be one of the possible environmentally friendly surface treatments for these materials.

In this work, the role of H_2O_2 in the formation of cerium-based conversion coatings was studied in detail at different concentrations on commercial carbon steel prepared by the immersion process. The relationship between the chemical and morphological changes induced by hydrogen peroxide and its protective properties were also analyzed. A possible mechanism is also proposed based on the results obtained in this work.

Experimental procedure

Coating preparation and characterization

Cerium conversion coating (CeCC) films were deposited on 10-mm thick specimens of AISI-1010 carbon steel (60 (100 mm), whose chemical composition was shown elsewhere [24]. Before depositing CCCs, the metal surface was mechanically grinded starting from coarse 240- to fine 1,000-grade emery papers, according to the standard metallographic techniques. In order to remove any remains of water or SiC due to the previous polishing of the samples, they were flushed out with acetone, distilled water, and dried at room temperature for 10 min. The cerium conversion treatments were performed by a simple immersion of the commercial carbon steel into different coating solutions containing 0.1, 1, and 10 g L^{-1} of CeCl_3 at 25 °C. In order to study the effect of the addition of H_2O_2 to the coating solution 3 mL of hydrogen peroxide per liter were added. The final pH of the solution was about 5.5. For comparison, the CrCCs were also deposited on AISI-1010 carbon steel specimens using a Chronak solution (200 g L^{-1} of $\text{K}_2\text{Cr}_2\text{O}_7$, and 5 mL of H_2SO_4). They were immersed in

the conversion bath at different times, ranging from 5 to 60 s, at room temperature. After treatment, the coated specimens were rinsed with deionized water and finally dried at room temperature.

Scanning electron microscopy and energy dispersive X-ray spectrometry (SEM/EDS) were employed to characterize the surface morphology of the cerium conversion coatings, using a JEOL JSM-35C equipped with a EDS voyager Tracor Northern Spectrometer. Electron accelerating voltages of 20 and 15 kV were used in backscattered electron and secondary electron investigation, respectively.

The crystallinity of the films was characterized by X-ray diffraction analysis, using a Siemens 5000 diffractometer, operating at 35 kV and 25 mA with a curved graphite crystal monochromator and a broad focus copper source. The samples were scanned at a speed of 2°min^{-1} and a range going from 15 to 100° .

Corrosion properties of the coatings

The corrosion performance was evaluated by electrochemical measurements, pull-off, and salt fog test. The electrochemical measurements were carried out at room temperature in NaCl (3 wt.%) using a conventional three-electrode cell. The solution was unstirred during the experiments and the pH of the solution was 6.1. The counter electrode was a large-area graphite bar. The reference electrode was a saturated calomel electrode, SCE (0.2415 V vs. SHE). The electrochemical measurements consisted of free-corrosion potential monitoring (E_{corr}), polarization resistance (R_p), and electrochemical impedance spectroscopy (EIS). The cell consisted of an acrylic rectangular box (60 (80(100 mm) and the exposed area of the sample was 0.785 cm^2 . The specimens were introduced by moderately pressing them against an o-ring, avoiding localized damage to the conversion layers. The R_p was evaluated from the linear polarization resistance (LPR) measurements according to the ASTM G-59-97 standard [25]. The coating resistance was analyzed by electrochemical impedance spectroscopy. The EIS measurements were carried out in the frequency region from 10,000 to 0.01 Hz (ten frequency points per decade) with an amplitude of 10 mV rms. In order to avoid any influence from previous polarization each measurement was taken from a new area of the sample.

For the adhesion strength and salt fog test, the samples were painted with a commercial polyurethane varnish (polyform 3000 COMEX) using a micrometric film aluminum applicator, obtaining a final dry film thickness between 40 and 45 μm , which was measured with a surface profiler (digital coating thickness gauge, Elcometer 345). The adhesion strength of the organic coatings on AISI-1010 commercial steel substrates, with and without chemical treatment, was measured with a C. C. Elcometer 106 series,

according to the ASTM D-4541 [26] standard. Aluminum studs, 21-mm diameter, were glued with epoxy resin onto the treated specimens for each test, followed by a deaeration process at room temperature during 24 h. The performance of cerium conversion coatings was also evaluated in neutral salt fog according to ASTM B-117 [27]. The salt spray (fog) test is often used to evaluate the relative corrosion resistance of coated and uncoated materials exposed to a salt spray or fog at an elevated temperature. The test specimens were placed in an enclosed salt spray cabinet or chamber and subjected to a continuous indirect spray of a neutral (pH 6.8) salt–water solution containing 5 wt.% NaCl. To exclude any possibility of contamination, fresh solution was used for each spray. Prior to the analysis an induced localized defect of 1 (50 mm in size) was made. This environment was maintained throughout the test. The water in the salt spray chamber was used according to the ASTM D1193 Specification for Reagent Water, Type IV; sodium chloride was added up to reach a 5% salt solution [28]. At the time the specimens were placed into the chamber, the cabinet was pre-conditioned to the operating temperature of 35 °C and fogging a 5% salt solution at the required of 12 mL h⁻¹. The default position for the sample placement was at a 25° angle from the vertical.

Results and discussion

Deposition time and microstructural characterization of spontaneous immersion coatings

In order to determine an adequate deposition time, open circuit potential (OCP) was evaluated in the cerate baths for 30 min and the results are shown in Fig. 1a, b. The equilibrium potential measurements for the coatings containing 0.1, 1, and 10 g L⁻¹ of CeCl₃ (free H₂O₂) are plotted versus immersion time and presented in Fig. 1a. From this figure, the OCP measurements were characterized by a strong initial decrease until approximately 10 min, followed by a much less severe decrease, and after 20 min, a fairly constant value was reached. As it can be observed, the evolutions are similar at the three concentrations but the OCP decay curves do not follow a clear trend from 0.1 g L⁻¹ towards 10 g L⁻¹. Even the interpretation of the OCP evolution during the conversion treatment becomes complex and should be done carefully, as Campestrini suggested [29], the cathodic or anodic displacement of the samples could be related to the reaction rate of the formation of a cerium layer. In addition to the aforementioned, the equilibrium potential is the condition at which the anodic and cathodic currents are equal, so its value depends on many variables, such as the rate of the anodic and cathodic reactions, or real anodic and cathodic

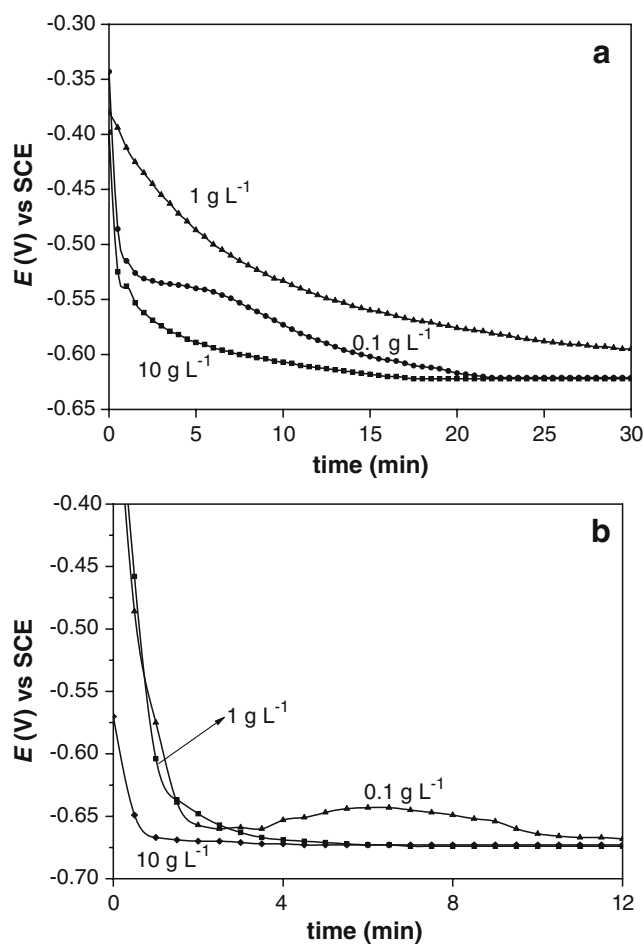


Fig. 1 Equilibrium potential measurements as a function of the immersion time in **a** CeCl₃ and **b** CeCl₃+H₂O₂ solutions

areas, which are often unknown [15–17, 30, 31]. Then, the initial sharp decrease is likely related to the activation of the surface, i.e. chemical thinning of the Fe oxide and/or chemical attack caused by the cerium baths, and may cause an increase in both the anodic current density and the anodic area. The thinning of the Fe oxide film results in an increase in the rate of the electrochemical reactions at the iron surface. It has been suggested that such an effect can be considered as a consequence of the increase in both the electron tunneling probability and metal migration, which may explain this trend as a function of cerium concentrations [32, 33]. Although from the results a stable potential is not obvious, it was considered that slow reaction rates to film formation were reached after 20 min.

The equilibrium potential was also monitored in cerium baths adding 3 mL per liter H₂O₂ to increase the deposition kinetics and the results are shown in Fig. 1b. First, it can be said that the open circuit potential was shifted to more negative potentials reaching an equilibrium potential in a short period of time. The presence of H₂O₂ caused heterogeneous coating deposition, leading to variations in

both the electrochemical activity and O_2 reduction reactions across the surface that influence coating deposition reactions. The reduction of hydrogen peroxide and oxygen in the proximity of the substrate caused an increase in the pH resulting in the precipitation of cerium hydroxide/oxide (pH \sim 6). The reduction reactions after the activation are likely to cause a higher decrease in the OCP observed after few minutes of conversion process. The deviation from the OCP behavior “shoulder” at $0.1 \text{ g L}^{-1} + H_2O_2$ may indicate that at this condition (immersion times between 3–10 min) the redox couple Ce (III)/Ce(IV) involved in the electrochemical process is interacting with the surface substrate increasing the OCP values. This potential in the $CeCl_3 + H_2O_2$ points out that in the cerate bath a cerium oxide protective film like CeO_2 and Ce_2O_3 could be formed inhibiting the substrate dissolution. From these analyses, the adequate immersion time to form cerium coatings was found of 20 and 10 min for specimens without and with H_2O_2 , respectively. In order to analyze the formation of chemical conversion treatments as functions of cerium concentration and the effect of H_2O_2 added to the conversion solutions, the specimens were analyzed by XRD and SEM.

The X-ray diffraction patterns of cerium coatings with added hydrogen peroxide are shown in Fig. 2. In this figure, the weak diffraction signals corresponding to crystalline CeO_2 and Ce_2O_3 can be seen. Additionally, iron oxide species (Fe_3O_4) have also been observed. The weak response resulted from some factors; thickness of the film, crystallite size, and substrate interference. However, a visual analysis of the samples indicated that after treatment, the conversion coating produced a significant surface color modification (pale yellow) that appeared uniform to the

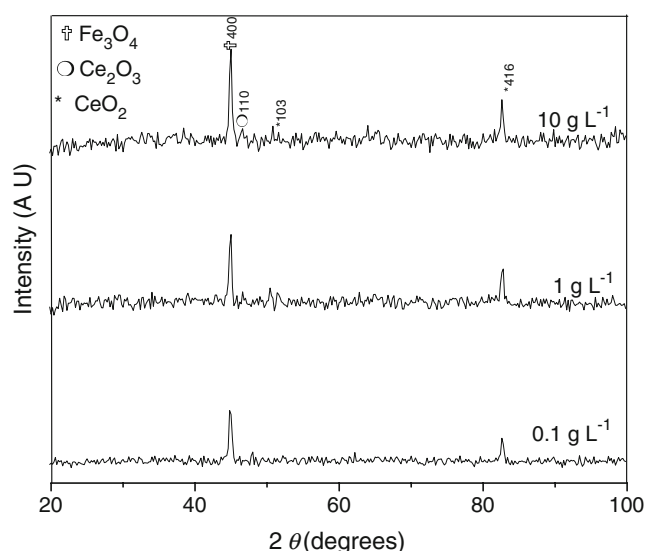
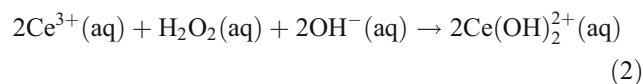
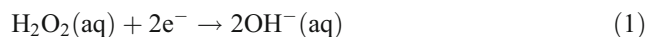


Fig. 2 XRD patterns of the samples treated in cerium solutions (a) $0.1 \text{ g L}^{-1} + H_2O_2$, (b) $1 \text{ g L}^{-1} + H_2O_2$, and (c) $10 \text{ g L}^{-1} + H_2O_2$

naked eye and may be related to the presence of cerium species on the surface substrate. The Ce and Fe quantity increases with the Ce-bath concentration.

Figure 3a–c shows the surface morphology of the Ce-based conversion coatings with H_2O_2 addition on AISI-1010 commercial steel samples. From the SEM images, the coatings formed on the carbon steel surface were inhomogeneous with visible roughness. The CeCCs are composed of agglomerated particles smaller than $0.5 \mu\text{m}$ in diameter where larger particles were dotted with smaller ones. The smaller particles seemed to correspond to rich cerium concentrations and appeared during the initial stages of the larger particles when the film is growing. These white randomly distributed semispherical deposits are composed by cerium oxides (high cerium and oxygen peaks), although the presence of some cerium hydroxide compounds (see the EDS analysis) cannot be discarded. Some superficial cracks with high cerium concentration are also visible in the micrographs. The SEM images indicate a higher compacticity with 0.1 g L^{-1} and 1 g L^{-1} (Fig. 3a, b) while at 1 g L^{-1} the surface displays a strong agglomeration in some areas (Fig. 3c). The deposit visual aspect in itself is also highly different with the cerium concentration, and it is increased when H_2O_2 is added. As a reference inset figures show the substrate surface of H_2O_2 -free CeCCs. By comparing the hydrogen peroxide effect on the deposition films, an increase in roughness, as the cerium-bath concentration is increased, can be observed.

The EDS analysis also showed that the immersion process of the AISI-1010 commercial steel in the cerium bath causes spontaneous dissolution of Fe at the local anodic sites and reduction of dissolved oxygen at local cathodic sites (Fig. 3a–c). The reduction of dissolved oxygen at local cathodic sites and the presence of H_2O_2 caused an increase in the pH of the solution above the solubility limit of solution cerium species, thereby favoring the precipitation of cerium oxide/hydroxide on the metal surface. In this substrate, H_2O_2 also plays an additional role as an oxidant, transforming Ce(III) to Ce (IV) in the solution, as it is described in the following equations:



Hughes et al. [31] reported that, during the cerium conversion process, the ceria particle size was increased with the immersion time. They suggested that the increase in the particle size was probably related to an increase in the pH near the surface because the rate of the hydrolysis of cerium ions is increased at a higher pH. Investigations on

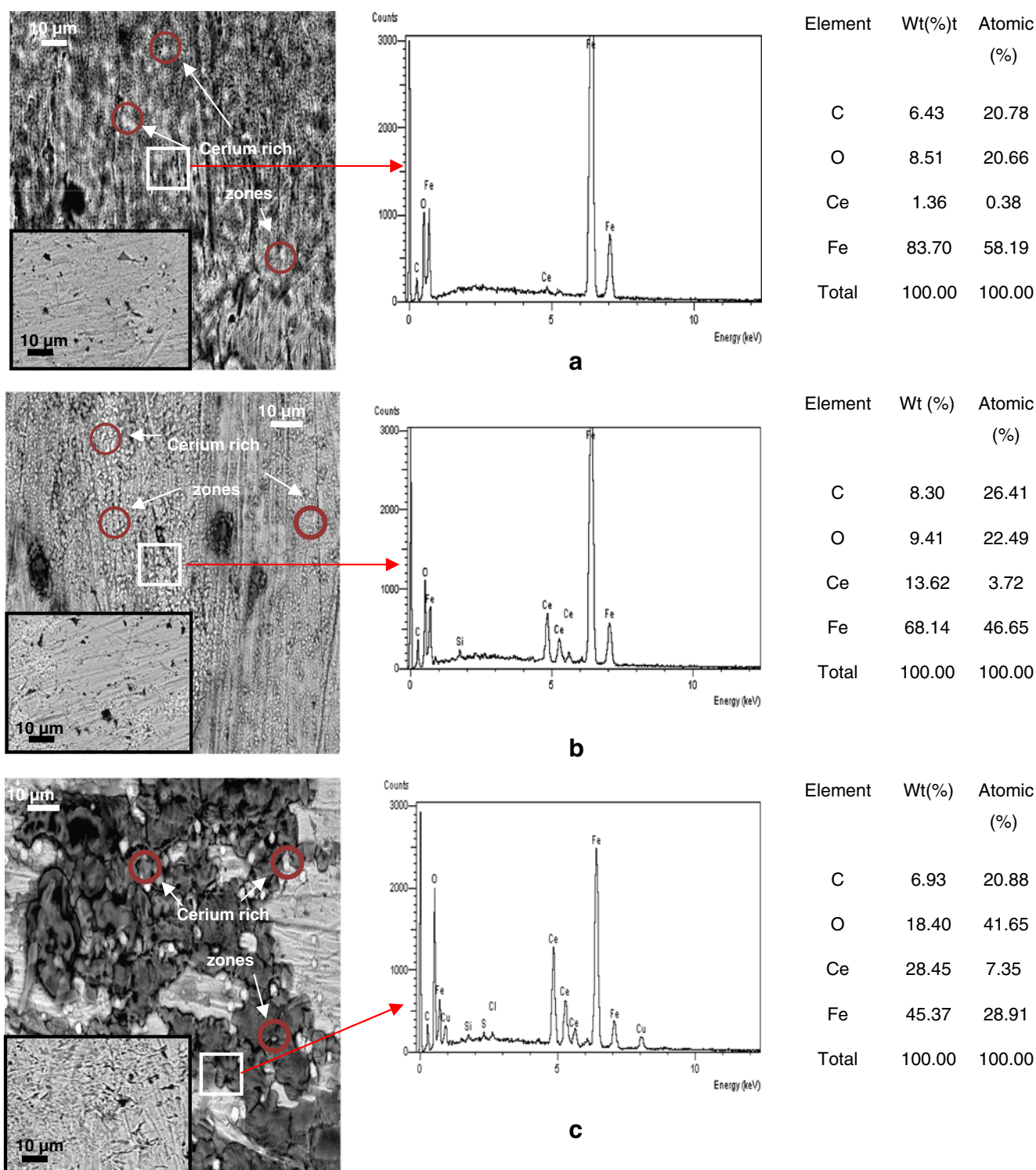


Fig. 3 SEM image of the surface morphology and the corresponding EDS analyses of cerium oxide conversion coatings deposited on AISI 1010 commercial steel after 10 min of immersion time in **a** 0.1 g L⁻¹, **b** 1.0 g L⁻¹, and **c** 10 g L⁻¹ of Ce-salt solution +H₂O₂ (3 mL per liter)

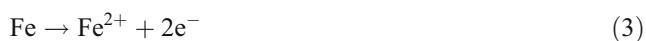
the preparation of CeO₂ powders for catalysis and ceramics have demonstrated that H₂O₂ exerts a significant influence on the properties of the formed precipitates such as crystallite size and tendency to agglomerate [34, 35]. Then,

in our study, the formation of coarse particles would be related to two factors, (1) an increase in the pH value of the hydroxide precipitation with the addition of H₂O₂ and (2) the amount of cerium ions due to the concentration of salts.

From the EDS analysis, it was confirmed that the Ce contents in the deposited films is increased with the cerium-bath concentration. White and gray agglomerates are rich in cerium and this can be attributed to the formation of cerium oxides, CeO_2 and Ce_2O_3 mainly, although, the presence of hydroxides like $\text{Ce}(\text{OH})_3$ cannot be discarded. Also Si and Cu no quantified during EDS analyses are observed, these elements seems to come from the substrate [24].

As it was shown in a previous characterization the growth of the cerium conversion films is strongly influenced by the addition of H_2O_2 . According to previous reports [31, 34, 35], the proposed mechanism, involving complexation of H_2O_2 with $\text{Ce}(\text{III})$ in the solution could be as follows: first when the carbon steel samples are in contact with the solution, the local pH is increased due to the reduction of dissolved molecular oxygen, according to the following equations:

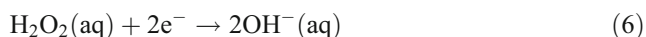
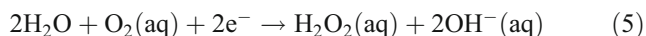
Anodic surface



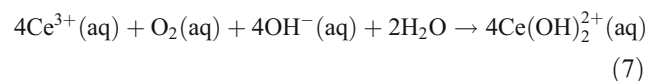
Cathodic surface



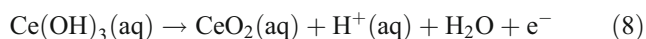
or



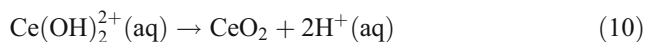
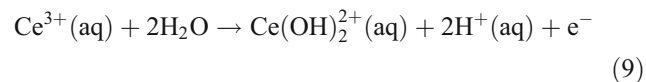
The results also demonstrate that H_2O_2 plays an important role in the conversion bath by inhibiting crystallization of CeO_2 in the absence of H_2O_2 ; the pathway for the formation of CeO_2 is via the $\text{Ce}(\text{OH})_4$ dehydration.



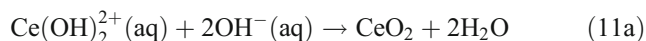
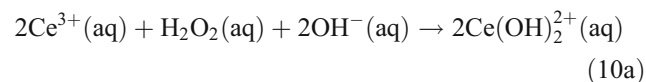
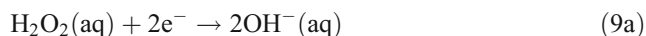
Conversely, when H_2O_2 is added to the solution, it catalyzes the production of OH^- ions, encouraging a faster precipitation of cerium ($\text{Ce}(\text{OH})_3$) in the cathodic areas by chemical reaction, followed by the formation of the CeO_2 protective layer.



A second pathway to CeO_2 can also be via the oxidation of Ce^{3+} ions to tetravalent $\text{Ce}(\text{OH})_2^{2+}$ and subsequent deprotonation, oxidation, and precipitation reactions.



or,



Thermodynamically, the formation of CeO_2 from $\text{Ce}(\text{OH})_3$ (Eq. 8) is more favored than that from $\text{Ce}(\text{OH})_2^{2+}$, besides the recorded OCP values and local pH are increased due to the reduction of dissolved oxygen and molecular hydrogen peroxide. In addition, during the conversion film formation, the substrate can be oxidized to produce lepidocrocite, which would be transformed into more stable oxides such as hematite and magnetite (Fe_3O_4) [36, 37]. In this case, the increase in pH can also favor adequate conditions to form magnetite, which, as it is well known promotes the adhesion of coatings [38, 39].

Corrosion properties of the coatings

E_{corr} measurements

The free-corrosion potential (E_{corr}) for cerium coatings with and without hydrogen peroxide was monitored in a 3 wt.% NaCl aqueous solution during 30 min and the results are shown in Fig. 4a, b. In general, the E_{corr} dropped below negative values as a result of the sudden creation of redox reactions on the films. After about 1 min of rapid drop, the E_{corr} was slowly decreased and tended to stabilize, mainly due to the formation of surface states such as cerium oxides (Fig. 4a). Eventually, steady states were attained with approximately unchanging E_{corr} values, owing to the balancing rate between reduction and oxidation reactions. It can also be seen that the relatively stable E_{corr} values at 20 min decreased with the increase in the peroxide-free cerium concentration. On the other hand, coated specimens with $\text{CeCl}_3 + \text{H}_2\text{O}_2$ displayed a corrosion potential that was lower than that observed in the bare steel samples and after 10 min the attained potentials were -620 , -661 , -662 , and -640 mV vs. SCE for 0, 0.1, 1, and 10 g L⁻¹, respectively (Fig. 4b). The E_{corr} evolution indicate that the CeCl_3 solutions are strongly influenced by the addition of H_2O_2 , affecting the kinetics of the reactions. Then in the evaluated solutions the electrochemical reactions are carried out in similar ways. Therefore, the $\text{Ce}^{3+}/\text{Ce}^{4+}$ redox couple was

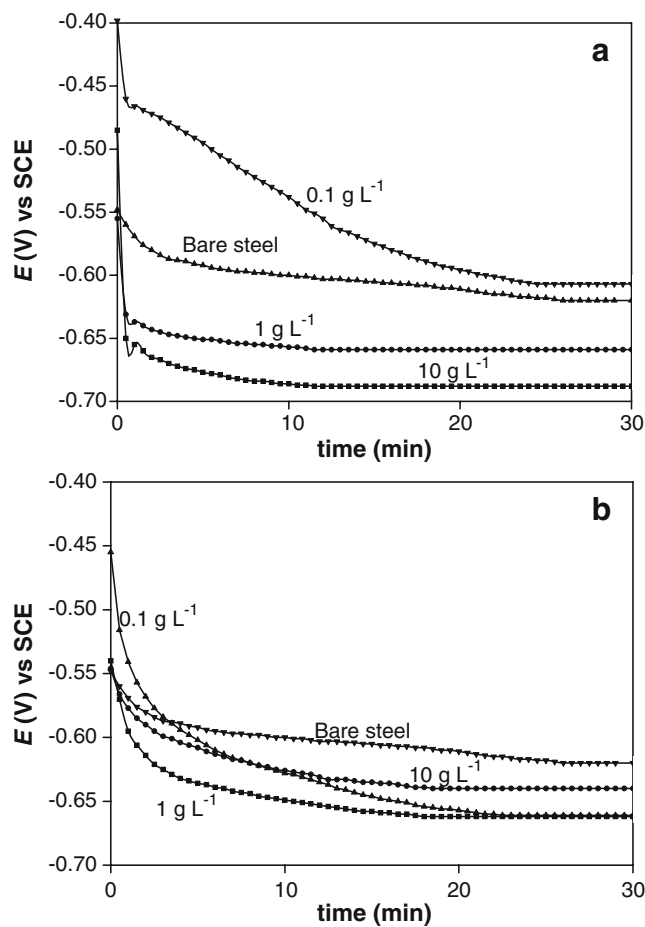


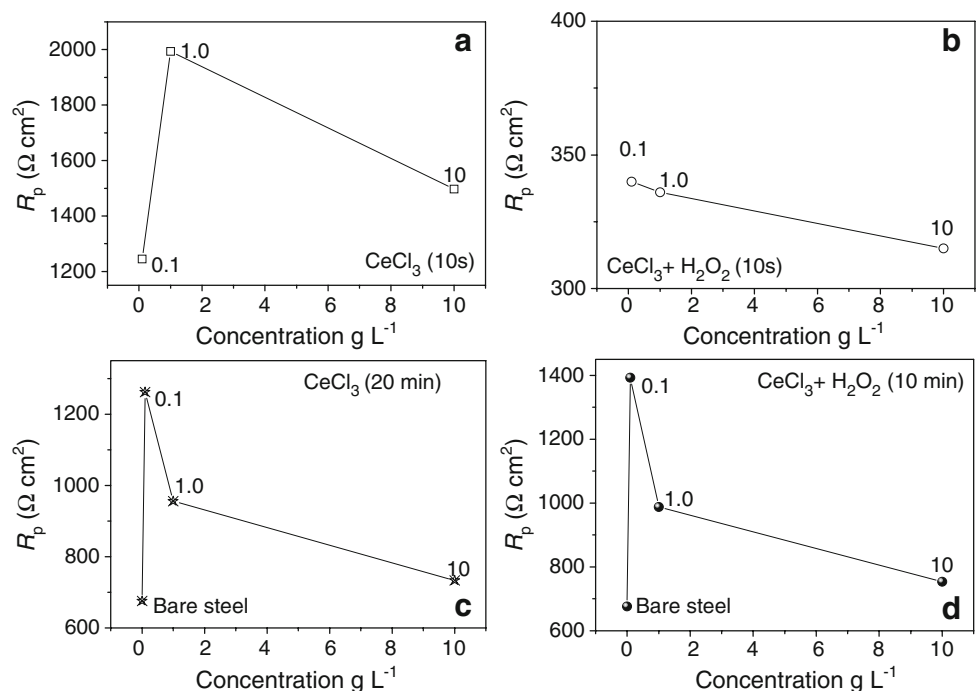
Fig. 4 Time vs. free-corrosion potential curves of the samples treated with **a** CeCl_3 and **b** $\text{CeCl}_3+\text{H}_2\text{O}_2$ baths using a NaCl (3 wt.%) aqueous solution

not directly involved in the electrochemical reactions on the Fe substrate as it is well known to be the case of the $\text{Cr}^{3+}/\text{Cr}^{6+}$ couple in the chromate conversion baths [40]. Though, the absence of a direct contribution of the $\text{Ce}^{3+}/\text{Ce}^{4+}$ couple does not necessarily exclude the oxidation by H_2O_2 of Ce^{3+} to Ce^{4+} . The constant potential reached in $\text{CeCl}_3+\text{H}_2\text{O}_2$ solutions pointed out that at the beginning the substrate was slightly attacked by the presence of hydrogen peroxide; but almost instantaneously, the cerium oxide film was formed, which could inhibit the corrosion substrate or promote the H_2O_2 reduction. Then, stronger reduction reactions after activation are likely to be the cause of the remarkable decrease in the equilibrium potential observed few minutes after the conversion process.

Polarization resistance (R_p)

In order to assess the protection degree afforded by the cerium coatings, the electrochemical behavior of the treated carbon steel specimens was studied by examining the linear polarization tests obtained in a NaCl (3 wt.%) aqueous solution. Such values are reported in Fig. 5a–d before and after the application of the protective treatment on the samples for different immersion times. The degree of protection has been evaluated by comparing the value of this resistance with that corresponding to an untreated sample. As it can be observed, with low immersion times (10 s) an important decrease in the R_p values can be observed when hydrogen peroxide is added (Fig. 5a–b). At this time, the solutions have no protective effects; even

Fig. 5 Dependence of R_p on cerium concentration and time of immersion in the cerium baths **a** 10 s (CeCl_3), **b** 10 s ($\text{CeCl}_3+\text{H}_2\text{O}_2$), **c** 20 min (CeCl_3), and **d** 10 min ($\text{CeCl}_3+\text{H}_2\text{O}_2$) in a NaCl (3 wt.%) aqueous solution



more, a decrease of R_p data was observed which was lower than that displayed by bare steel. The negative effect with this time of treatment can be understood by an initial attack on the substrate surface and the fact that the protective film was not still formed. On the other hand, the obtained R_p values of the samples treated during 10 min of immersion ($\text{CeCl}_3 + \text{H}_2\text{O}_2$) were slightly higher than those of the samples coated with CeCl_3 for 20 min (Fig. 5c–d). Then, the H_2O_2 addition results in the deposition of conversion layers at much faster rates (~10 min) giving similar protective effects on this substrate, even though the polarization resistance values only increased twice with respect to those showed by bare steel.

For comparison purposes, chromium conversion layers at different immersion times (5, 10, 30, and 60 s) were also synthesized and evaluated in an aggressive medium (Fig. 6a–b). From these curves, the chromium conversion baths produced at 5 s displayed a R_p ($1,500 \Omega \text{ cm}^2$) higher than that obtained at 10, 30, and 60 s, and a positive

displacement in the E_{corr} can be observed (–630 mV). Even though cerium baths displayed a similar electrochemical behavior the passive film observed in chromate solutions, it is well known that chromate ions play a fundamental role in the formation of passive films inhibiting the aggressiveness of the corrodent by a noble shift of the corrosion potential [41, 42].

In addition to the aforementioned, it has also been reported [43, 44] that the corrosion performance of the conversion coatings depends on both the coating properties and the substrate. It is worth mentioning that the synergistic effects between the CrCCs and substrates, results in an increase in the overall chromium (VI) content in the coating. From previous reports and the results discussed above, it can be suggested that the chromate coatings resulted in the formation of more protective barriers, but the Ce treatments in the presence of H_2O_2 seems to be an alternative to avoid the corrosion of this carbon steel.

EIS

Nyquist and Bode plots of the treated samples in solutions containing $\text{CeCl}_3 + \text{H}_2\text{O}_2$ and evaluated in an aggressive environment (NaCl) are shown in Fig. 7a–b. As a reference, bare steel was also analyzed during the EIS measurements. The inset Fig. 7a shows the equivalent circuit used to fit the parameters and the values are listed in Table 1. The simulation points originated from the fitting process are also given in Fig. 7a, b (continuous line). The intersection of capacitive loop with the real axis represents the resistance charge transfer, R_{ct} or resistance of the CeCCs, R_p , and the solution enclosed between the working electrode and the reference electrode, R_s . R_{ct} and R_p represent a measure of the electron transfer across the surface and are inversely proportional to the corrosion rate. The constant phase element, CPE, is introduced in the circuit instead of the pure double-layer capacitor to give a more accurate fit. The impedance of the CPE is expressed as:

$$Z_{\text{CPE}} = \frac{1}{Y_o(j\omega)^n} \quad (12)$$

Where Y_o is the magnitude and n is the empirical exponent of the CPE, $0 \leq n \leq 1$. Nyquist diagrams show one depressed loop with real impedances ranging between 156 and $1,419 \Omega \text{ cm}^2$ in the spectra, whereas impedances from 62 to $310 \Omega \text{ cm}^2$ are observed in the imaginary part. The real and imaginary impedances are inversely affected by the amount of cerium. From the Nyquist plot, it is clear that the treated samples with cerium baths containing 0.1 g L^{-1} displayed impedance values only twice higher than those showed by the bare steel (Table 1). However, the specimens

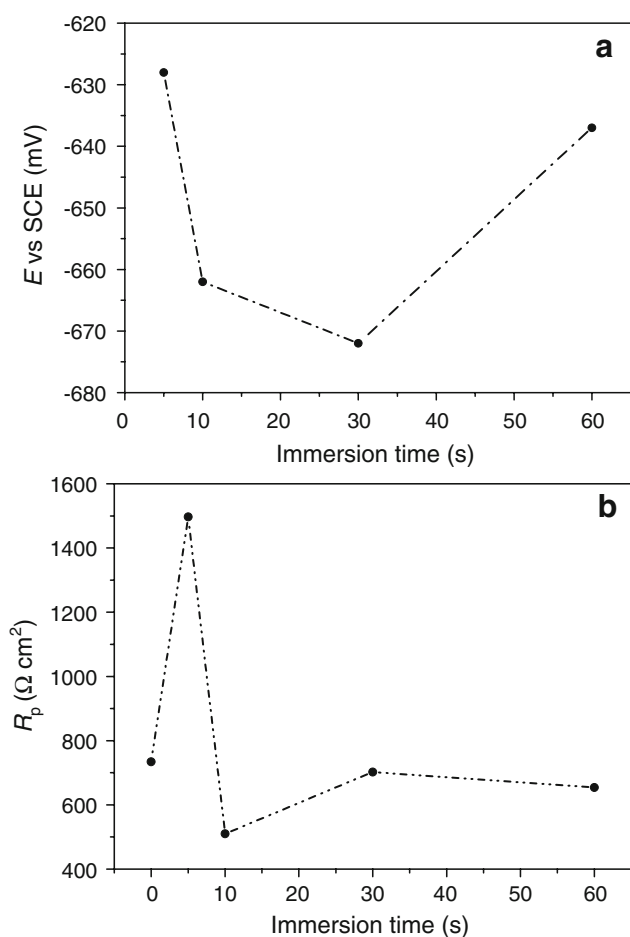
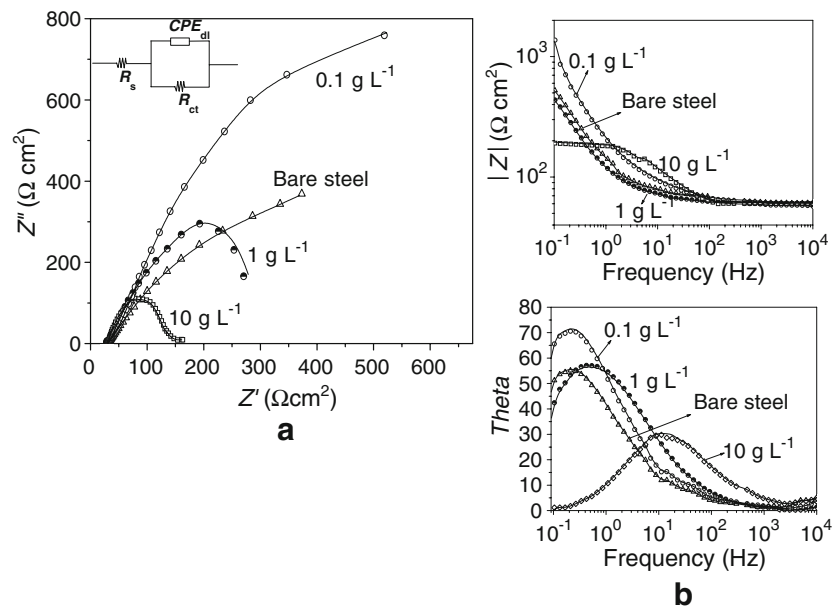


Fig. 6 **a** E_{corr} evolutions and **b** polarization resistance curves obtained from the treated samples in Chronak solutions at different immersion times (0, 5, 10, 30, and 60 s) and evaluated in a NaCl (3 wt.%) aqueous solution at room temperature

Fig. 7 **a** Nyquist and **b** Bode plots for treated and untreated samples at different cerium salt concentrations (0.1, 1 and 10 g L⁻¹ +H₂O₂)



treated in solutions containing 1 and 10 g L⁻¹ of cerium did not show additional protective properties. On the contrary, it seems that with these cerium concentrations the corrosion rate was increased. The increase for low cerium concentrations suggests that a protective conversion layer is formed with cerium species, mainly hydrated oxides that act as a real barrier against the penetration of ions from the solution.

The differences in the electrochemical behavior of the samples can also be observed in the Bode plots. First of all, although all the specimens, including bare steel, showed a similar behavior, the conversion-coated samples with cerium contents of 0.1 g L⁻¹ exhibited the highest phase angle (71°). More detailed investigations performed by other authors on chromate conversion coatings using aluminum alloys as a substrate ascribed the existence of this time constant to the coating itself, which could be the case of the dissolutions investigated in this work [6, 31]. The relationship between the time constants and the interfacial charge transfer phenomena, and the clear displacement of the phase angle observed at lower

frequencies in the conversion films, may indicate a hindrance to these phenomena by the presence of the conversion layers (0.1 g L⁻¹); i.e., the time constants associated with the corrosion process have been displaced to even lower frequencies due to this conversion layer. The corrosion resistance obtained at low cerium concentrations can also be attributed to the insulation of the substrate in the corrosive medium, inhibiting the free diffusion of oxygen or Cl⁻ ions. Research works have revealed that Ce treatments on different substrates increase the anticorrosive properties as cerium concentration is increased [13, 15, 23, 25]; however, in our electrochemical results, enhanced properties were only reached at low cerium concentrations and lost when cerium concentration is increased, which could suggest a different attack pathway on AISI-1010 commercial carbon steel. The apparent contradiction with previous results reported in the literature [22, 45] is also explained in terms of surface preparation which strongly influences the formation of homogeneous CCCs and affects the protection properties. Additionally, some differences in the operational parameters like kind of substrate (intermetallic compounds present during the CeCCs), deposition duration, and bath temperature should be considered in the corrosion behavior of the carbon steel samples, which may alter the number and distribution of cathodic sites on the surfaces and influence the deposition of the cerium conversion coating, including its uniformity, thickness, morphology, and adherence to the substrate [46, 47]. Comparing electrochemical responses obtained during linear polarization and EIS methods, some differences in the R_p values were observed. However, the trend seems to remain the same. Coated samples with 0.1 g L⁻¹ +H₂O₂ presented an increase in the corrosion resistance while the

Table 1 Fitted results obtained from the EIS spectra of pre-treated samples in a NaCl (3 wt.%) aqueous solution

Sample	R _s (Ω cm ²)	CPE _{dl}		R _{ct} (Ω cm ²)
		Y ₀ (F cm ⁻²)	n	
Bare steel	29.2	3.50 × 10 ⁻³	0.77	656.4
0.1 g L ⁻¹	30.2	2.79 × 10 ⁻³	0.67	1,419.8
1.0 g L ⁻¹	30.8	5.50 × 10 ⁻³	0.69	356.5
10.0 g L ⁻¹	29.1	6.24 × 10 ⁻⁴	0.74	156.5

treated samples with 1 and 10 g L⁻¹ were far from this behavior. The differences can be explained in terms of the limits in each technique; whereas the impedance involve the conversion of time-domain input–output signals into a complex quantity that is a function of frequency, the LPR measurements provide a method to rapidly identify corrosion upsets but cannot provide information on the RC time constants of the electrochemical processes.

Continuous immersion tests

To follow the previous characterization of the uncoated substrates is very important to understand the behavior of fully coated systems, since the final product is usually painted. Moreover, this is the main interest in industrial applications. The characterization of these systems is very important, and two aspects can be analyzed: the barrier effect of the paint and the role of the pre-treatment on the corrosion behavior of the coated substrate. It is known that in the absence of defects the coating essentially behaves as a physical barrier between the aggressive electrolyte and the metal. Usually a very good coating (uniform and thick) behaves as an insulator showing very high resistance (GΩ cm²) [48]. Moreover, very low capacitances are usually obtained and the phase angle of the impedance plots is around -90° over the measured frequency range. In this situation a long time of exposure is necessary to allow corrosion onset. For this reason, in the present work a low quality organic coating was used in order to reduce the experiment time and facilitate the access of aggressive species to the metallic substrate and thus understand the role of the pre-treatments in the presence of paint coating. Despite the low quality of the coating, the evaluation was carried out at least during 5 days of immersion; Fig. 8a, b depict the Nyquist and Bode plots for bare steel used as a reference and cerium concentration of 0.1 g L⁻¹ +H₂O₂. It must be remembered that the impedance spectrum was divided into two parts: the high-frequency part that is related to the organic coating while the low-frequency (LF) part corresponds to the reactions occurring on the metal through defects and pores in the coating. In the very LF range <200 mHz, the points are more scattered due to the high impedance of the system and some of them are not reported in the figures.

The electrochemical equivalent circuits and fitted values of the different samples after application of top-coat (40 μm of organic film) as a function of the immersion time are reported in Table 2. In this case, R_s is the solution resistance, R_{coat} is the organic coating resistance while CPE_{coat} models the intact layer, R_{ct} is the charge transfer resistance and CPE_{dl} models the double charge layer capacitance, R_{ox} and CPE_{ox} are the resistance and capacitance of the conversion layer; Y_0 is the capacitive

admittance and n is the empirical exponent of the CPE. From the EIS results, it can be seen that immersion time exerts a significant effect on the impedance of the samples, which helps to understand the effects of the different pre-treatments. Initially ($t=0$ h), the bare steel shows the presence of a time constant from intermediate to high and low frequency regions (Fig. 8a) with a high coating resistance ($3.38 \cdot 10^7 \Omega \text{ cm}^2$), $Y_{\text{o,coat}}=3.54 \cdot 10^{-10} \text{ F cm}^{-2}$ and $n=0.94$. However, only after 1 h of immersion, the samples showed an important decrease in the total impedance values up to $3.68 \cdot 10^6 \Omega \text{ cm}^2$, $Y_{\text{o,coat}}$ increased to $6.23 \cdot 10^{-10} \text{ F cm}^{-2}$ and $n=0.89$. At this stage a second time constant appeared, and it can be considered as a representative of the diffusion process of oxygen through the coating. As for the samples immersed for 24 h, the Nyquist plots are characteristic in two parts. At high frequencies, the response is purely capacitive and it is due to the presence of the organic coating. However, at low frequencies the phase angle starts to increase as a consequence of the ingress of the electrolyte in the paint film (diffusion by porous film). This could indicate that the paint already presents conductive pathways whereby water and active species penetrate. These time constants were relatively small and the impedance values decreased until $1.20 \cdot 10^6 \Omega \text{ cm}^2$ and $1.18 \cdot 10^6 \Omega \text{ cm}^2$ for the coating and charge transfer resistance, respectively. For 48 h of immersion, the first time constant began to disappear and only one big arc could be seen in the plot. Some Fe corrosion products, which appeared uniform, were observed on the surface substrate, then, this new time constant could reflect information of the substrate (commercial steel). So we do believe that the corrosive medium reached the substrate surface. When the immersion time exceeded 72 and 96 h, only one time constant with an important increase in the total impedance was observed ($7.03 \cdot 10^6$ and $7.11 \cdot 10^6 \Omega \text{ cm}^2$). The visual aspect of these samples was reddish-ochre and the chemical analysis of the film formed on the bare steel indicated that the products were mainly composed of magnetite and lepidocrocite [24]. So, the former barrier caused an increase in the total impedance values, which was perfectly observed after 72 h; although it is necessary to consider that the passive film is regularly not stable and with poor adhesion properties. The entire deterioration process of the organic coating and formation of corrosion products could be divided into three main stages. (1) Medium penetrating through coating, (2) medium reaching metal surface causing corrosion, and (3) corrosion expansion (formation of corrosion products) resulting in coating delamination [49].

In the case of the coated specimens after Ce baths and short immersion times (24 h), the impedance plots present a linear region in the high-frequency region, which means that the film behaves like a blocked electrode (Fig. 8b). The

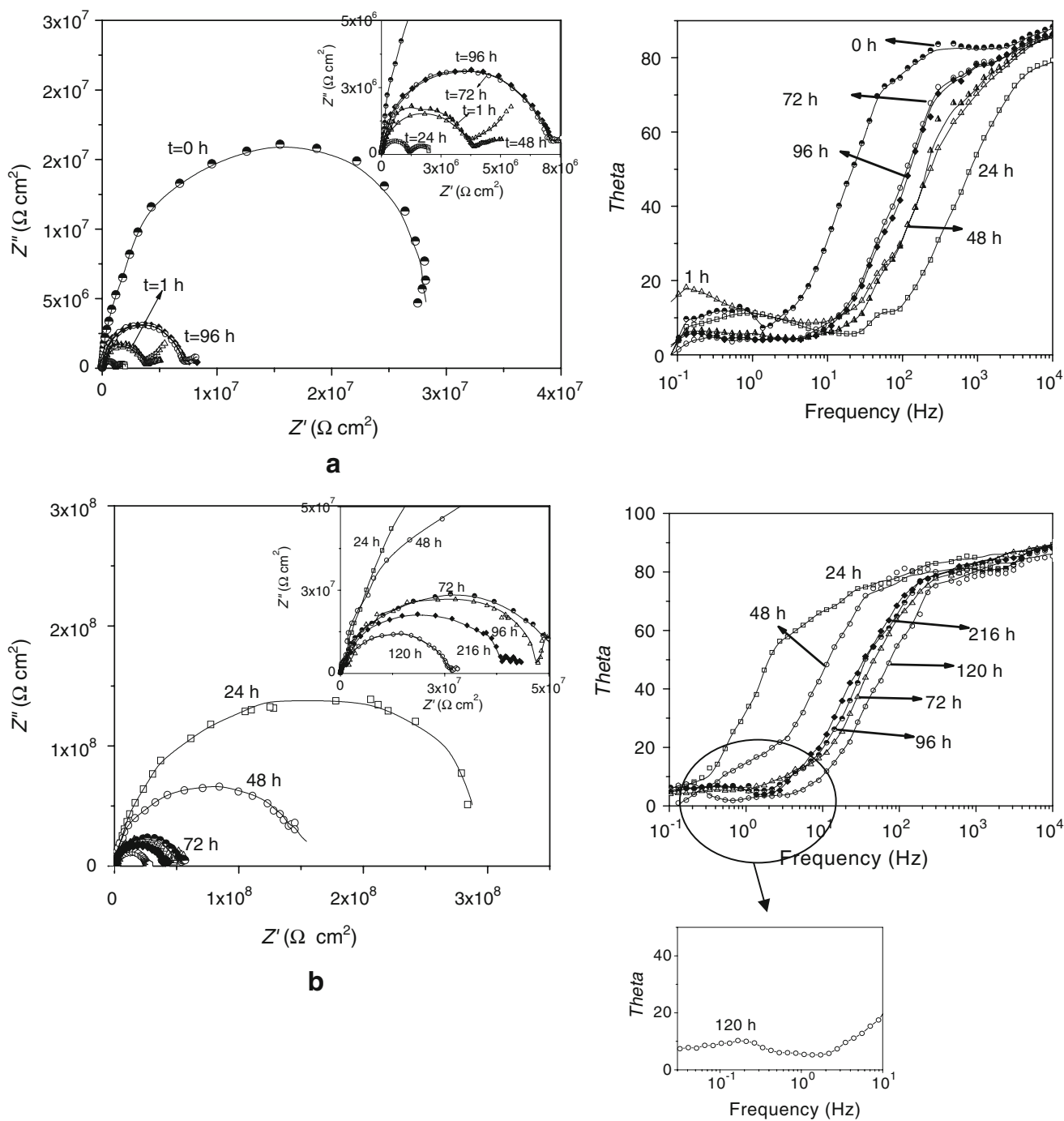
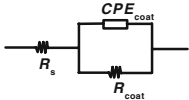
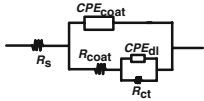
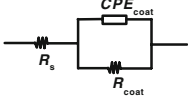
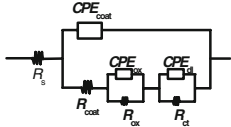


Fig. 8 Nyquist and phase angle diagrams for **a** bare steel coated with a polyurethane varnish, **b** after Ce-treatment ($0.1 \text{ g L}^{-1} + \text{H}_2\text{O}_2$) + coated (polyurethane varnish), evaluated in continuous immersion in a NaCl (3 wt.%) aqueous solution

plots show a resistive response ($R_{\text{coat}} 3.28 (10^8 \Omega \text{ cm}^2)$, which at this stage can be assigned to the organic coating resistance. These values are in good agreement with the impedance and capacitance values of a film reported elsewhere but with a thickness about $80 \mu\text{m}$ [50]. When the time of exposure in the aggressive medium is increased, the diagrams were gradually reduced in the total impedance

up to $2.64 (10^7 \Omega \text{ cm}^2)$ after 120 h. At this stage, the total impedance of the samples was about 12 times below the initial one. In spite of this, it is appreciable the diminution in the coating resistance, and the conversion layer provides a degree of protection that is higher than that observed in bare steel. This behavior results from the fact that the cerium film helps in the adhesion of the coating and

Table 2 Fitted parameters of the different samples after application of top-coat (40 μm of organic film) as a function of immersion time in a NaCl (3 wt.%) aqueous solution

Bare steel								
Immersion Time (h)	R_s ($\Omega \text{ cm}^2$)	CPE_{coat}		R_{coat} ($\Omega \text{ cm}^2$)	CPE_{dl}		R_{ct} ($\Omega \text{ cm}^2$)	Equivalent circuit
		Y_o (F cm^{-2})	n		Y_o (F cm^{-2})	n		
0	31.23	3.54×10^{-10}	0.94	3.38×10^7	-	-	-	
1	30.57	6.23×10^{-10}	0.89	3.68×10^6	3.31×10^{-7}	0.62	4.38×10^6	
24	30.62	5.61×10^{-10}	0.90	1.20×10^6	4.19×10^{-7}	0.63	1.18×10^6	
48	29.13	3.80×10^{-10}	0.94	3.80×10^6	3.86×10^{-7}	0.54	2.01×10^6	
72	30.14	3.96×10^{-10}	0.93	7.03×10^6	3.20×10^{-7}	0.60	1.28×10^6	
96	30.40	4.17×10^{-10}	0.94	7.11×10^6	2.62×10^{-7}	0.61	2.23×10^6	
0.1 g L ⁻¹ Ce + 3 mL H ₂ O ₂								
Immersion Time (h)	R_s ($\Omega \text{ cm}^2$)	CPE_{coat}		R_{coat} ($\Omega \text{ cm}^2$)	CPE_{ox}		R_{ox} ($\Omega \text{ cm}^2$)	Equivalent circuit
		Y_o (F cm^{-2})	n		Y_o (F cm^{-2})	n		
24	30.43	1.61×10^{-10}	0.92	3.28×10^8	-	-	-	
48	30.27	1.46×10^{-10}	0.93	1.53×10^8	-	-	-	
72	30.45	1.86×10^{-10}	0.90	4.75×10^7	-	-	-	
96	29.13	1.62×10^{-10}	0.92	4.66×10^7	-	-	-	
120	30.43	1.37×10^{-10}	0.93	2.64×10^7	2.32×10^{-7}	0.64	2.10×10^6	
216	30.62	1.65×10^{-10}	0.92	4.08×10^7	2.63×10^{-7}	0.66	5.43×10^6	

increase corrosion protection, preventing water and aggressive species from reaching the metallic interface. The observed changes in the values fitted from the EIS spectra using different equivalent circuits such as coating resistance, coating capacitance, resistance of conversion and capacitance of conversion layer, charge transfer resistance, and double-layer capacitance indicate the features of the deterioration process of the organic film and the protection of the conversion layer. After 120 h of immersion, the Nyquist and Bode plots exhibit a well-defined arc and a second begins to form at low frequency regions (see inset figures). The first arc is relatively larger ($2.64 (10^7 \Omega \text{ cm}^2)$) and the second is relatively smaller ($2.10 (10^6 \Omega \text{ cm}^2)$). This indicates that the outer layer of the system (organic coating) begins to lose its anticorrosive properties; however, the

magnitude of the resistance points out that the corrosion medium is still blocked by the cerium conversion layer during its permeating to the substrate. After 216 h, the EIS plots show an increase in the impedance values, which reflects the information of the corrosion process on the substrate surface. At this step the oxide/hydroxide cerium compounds still already permeated into the outside of the substrate and the corrosion spread out sealing the surface.

Considering the impedance values exhibited by the conversion-coated carbon steel samples, it must be said that they were much lower than those exhibited by other authors for Al alloys covered with CeCl_3 [15, 16, 22, 23, 45, 51]. However, they are comparable to the protection offered by chromate conversion coatings on the same substrate in a NaCl solution discussed above. Furthermore,

Table 3 Pull-off results

Sample	Bond strength values (MPa)
Bare steel	1.5±0.08
0.1 g L ⁻¹ +H ₂ O ₂	3.5±0.15
1 g L ⁻¹ +H ₂ O ₂	2.5±0.12
10 g L ⁻¹ +H ₂ O ₂	1.7±0.11
Chromate treatment	3.2±0.13

if we analyze the values obtained for both the bare steel and treated samples we can see an increase (up to an order of magnitude) in the total impedance values when the chemical treatment is applied, at the beginning, from 3.3 (10⁷ Ω cm² to 8.5 (10⁹ Ω cm², and after 96 h of continuous immersion from 7.11 (10⁶ Ω cm² to 4.66 (10⁷ Ω cm².

Pull off and salt fog tests

The bonding strength of cerium pre-treatments on commercial carbon steel was examined by a pull-off test, and the values shown in Table 3 are the average of five tests. By taking into account the equilibrium potential measurements, only the treated samples with different cerium concentrations in H₂O₂ presence and 10 min of immersion time were evaluated.

The bonding strengths were approximately 3.5±0.15, 2.5±0.12, and 1.7±0.11 MPa for cerium salt concentrations of 0.1, 1, and 10 g L⁻¹, respectively, while the results for

bare steel were about 1.5±0.1 MPa. The heterogeneity of the film developed on the substrate was increased with the concentration and fracture occurred inside the films but not at the interface, therefore, the paint was almost completely removed from the substrate (around a 90% blistered area), which confirms the role of the pre-treatments as precursors of adhesion. Table 3 also shows bond strength data for chromium conversion treatments after 5 s of immersion. From the table, it is seen that this bonding strength is comparable with low concentrations of cerium, which is even higher than that for chromate conversion treatments.

The results suggest that the adhesion properties between the polymer varnish and AISI-1010 commercial steel substrate were improved by using cerium baths at low concentrations. The decrease in the adherence for 1 and 10 g L⁻¹ could be associated to the surface attack during the chemical treatment, which was observed by SEM measurements (Fig. 3a–c). This attack causes a larger surface roughness but a weak adherence, which affects the bonding performance among the different interfaces.

The corroded surface morphology of the treated sample after a 120 h salt fog testing is shown in Fig. 9a–c [27]. The red rust characteristic of the corrosion process is clearly observed and as a consequence of the defect induced into the samples, the access of water, chloride ions, and oxygen was favored, allowing an increase in the corrosion rate in this zone. However, no areas of the coating peeled away. As it is the case for 1 and 10 g L⁻¹ (Fig. 9b, c), the samples were severely corroded and deep corrosion can be seen on the surface at 0.1 g L⁻¹ (Fig. 9a). Then, hydrogen peroxide

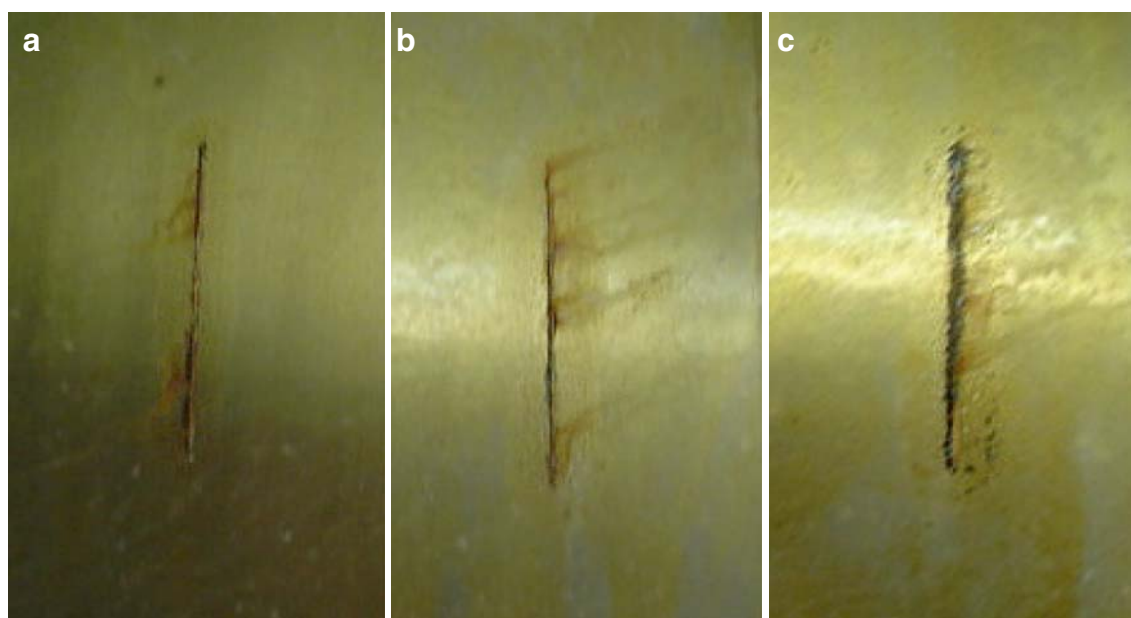


Fig. 9 Visual aspects of the pre-treated samples at different concentrations of CeCl₃+H₂O₂ (3 mL per liter) solutions after 120 h of salt fog evaluation **a** 0.1 g L⁻¹, **b** 1.0 g L⁻¹, and **c** 10 g L⁻¹ of cerium

accelerates the oxygen–cerium combination process to form a thin and rough protective oxide film on the surface, improving the adhesion properties and mitigating the corrosion to a certain extent of time at low concentrations of cerium salt.

Conclusions

Chromium-free conversion coatings on carbon steel were obtained by using different aqueous baths of cerium salts in presence of H_2O_2 , and their corrosion resistances were compared with the one performed by a chromate protective coating. The influence of H_2O_2 on deposition films was observed at different concentrations, which favors the precipitation of cerium oxide/hydroxide on the metal surface and an increase in roughness as the cerium bath concentration is increase. In addition, hydrogen peroxide can help to obtain coatings with enhanced corrosion resistance, adhesion strength properties, and reduced immersion times. Then, during the coating deposition H_2O_2 acts as a complexing agent, oxidant, or a source of OH^- ions leading to precipitation reactions that increase the local pH. The comparison between the investigated concentrations reveals that cerium conversion treatments can be efficient at low concentrations, hindering delamination of painted steel substrates immersed in chloride containing media. This effective protection against corrosion is the result of the combination of both good adhesion to metal substrates and barrier properties. The EIS results fitted well with the different proposed equivalent circuits which were adjusted as functions of immersion time, considering that the high-frequency part is related to the organic coating while the low-frequency part corresponds to the reactions occurring on the metal through defects and pores in the coating and displays the information of the corrosion process on the substrate surface, which changes from a slow process with the resistance, gradually decreasing to a fast transition period with the EIS changing from the single capacitive loop to double capacitive loops and finally a relatively stable process controlled by oxygen diffusion.

Acknowledgments The authors wish to acknowledge the financial support given by UNAM through the DGAPA PAPIIT IN 115603-project, DGAPA-UNAM, and CONACYT through the 61354 project. The authors would like to thank Mr. Ivan Puente L. for the SEM analyses.

References

- Neri W (1990) *Introduzione alla Verniciatura delle superfici metalliche* 3rd edn. Tecniche Nuove, Milan
- Xinweng Y, Chunan C, Zhiming Y, Derui Z, Zhongda Y (2001) *Corros Sci* 43:1283
- Horn K, Krause S, Weinberg G, Bange K (1987) *Thin Solid Films* 150:41
- Arnott DR, Hinton BRW, Ryan NE (1989) *Corros* 45:12
- Schram T, Goeminne G, Terryn H, Van Hoolst W, Van Espen P (1995) *Trans Inst Met Finish* 73:91
- Fedrizzi L, Deflorian F, Bonora PL (1997) *Electrochim Acta* 42:969
- Zhang W, Li JQ, Wu YS, Xu JT, Chen K (2002) *Surf Eng* 19:224
- Hinton BRW, Arnott DR, Ryan NE (1986) *Mater Forum* 9:162
- Mansfeld F, Shih H, (1990) In: *Proceeding of the conference on 11th International Corrosion Congress, Florence, Italy, A I M* 4555
- Hughes AE, Hardin SG, Harvey TG, Nikour T, Hinton B (2003) *ATB Metallurgie* 43:264
- Rivera BE, Johnson BY, O'Keefe MJ, Fahrenholtz WG (2004) *Surf Coat Technol* 176:349
- Wang C, Jiang F, Wang F (2004) *Corros* 60:237
- Brunelli K, Dabala M, Calliari I, Magrini M (2005) *Corros Sci* 47:989
- Ardelean H, Fiaud C, Marcus P (2001) *Mater Corros* 52:889
- Mora N, Cano E, Polo JL, Puente JM, Bastidas JM (2004) *Corros Sci* 46:563
- Böhm S, Greef R, McMurray HN, Powell SM, Worsley DA (2000) *J Electrochem Soc* 147:3286
- Aramaki K (2004) *Corros Sci* 46:1565
- Pourbaix M (1974) *Atlas of electrochemical equilibria in aqueous solutions*. National Association of Corrosion Engineers, Houston
- Hayes SA, Yu Pu, O'Keefe TJ, O'Keefe MJ, Stoffer JO (2002) *J Electrochem Soc* 149:623
- Davenport AJ, Isaacs HS, Kendig MW (1991) *Corros Sci* 32:653
- Dabala M, Ramous E, Magrini M (2004) *Mater Corros* 55:381
- Dabala M, Armelao L, Buchberger A, Calliari I (2001) *Appl Surf Sci* 172:312
- Scholes FH, Soste C, Hughes AE, Hardin SG, Curtis PR (2006) *Appl Surf Sci* 253:1770
- Onofre-Bustamante E, Domínguez-Crespo MA, Genescá-Llongueras J, Rodríguez-Gómez FJ (2007) *Surf Coat Technol* 201:4666
- Standard practice for: conducting potentiodynamic polarization resistance measurements (2003) ASTM G59-97, American society for testing and materials, West Conshohocken, PA
- Standard practice for: pull-off strength of coatings using portable adhesion testers (1995) ASTM D4541-95, American society for testing and materials, West Conshohocken, PA
- Standard practice for: operating salt spray (fog) apparatus (1997) ASTM B117-97, American society for testing and materials, West Conshohocken, PA
- Standard practice for: Standard specification for Reagent Water (2006) ASTM D1193-06, American society for testing and materials, West Conshohocken, PA
- Campestrini P, Terryn H, Hovestad A, de Wit JHW (2004) *Surf Coat Technol* 176:365
- Aldykiewicz AJ, Isaacs HS, Davenport AJ (1995) *J Electrochem Soc* 142:3342
- Hughes AE, Gorman JD, Miller PR, Sexton BA, Paterson PJK, Taylor RJ (2004) *Surf Interface Anal* 36:290
- Shimizu K, Brown GM, Kobayashi K, Thompson GE, Wood GC (1993) *Corros Sci* 34:1853
- Dignam MJ, in Diggle JW (Ed) (1972) *Oxide and oxide films*, 1. Marcel Dekker Inc, New York, Ch 2
- Djuricic B, Pickering S (1999) *J Eur Ceram Soc* 19:1925
- Lee JS, Choi SC (2004) *Mater Lett* 58:390

36. Mariaca Rodríguez L, Genescá Llongueras J, Uruchurtu Chavarin J, Hernández L (1999) *Corrosividad atmosférica (MICAT-MÉXICO)*. Plaza y Valdes, México
37. Molera Sola P (1989) *Recubrimientos de los metales*. Marcombo, Barcelona
38. Leeds JM, Grapiglia J (1995) *Corros Prevent Control* 42:77
39. Goemine JG, Terryn H, Vereecken J (1998) *Electrochim Acta* 43:1829
40. Aldykiewicz AJ, Davenport AJ, Isaacs HS (1996) *J Electrochem Soc* 143:147
41. Cheng YF, Luo JL (1999) *Electrochim Acta* 44:4795
42. Cheng YF, Luo JL (2000) *Appl Surf Sci* 167:113
43. Abd El Aal EE, Abd El Aal A, Abd El Haleem SM (1994) *Corros Meth Mater* 41:4
44. Long ZL, Zhou YC, Xiao L (2003) *Appl Surf Sci* 218:123
45. Bethencourt M, Botana FJ, Cano MJ, Marcos M (2002) *Appl Surf Sci* 189:162
46. Arurault L, Monsang P, Salley J, Bes RS (2004) *Thin Solid Films* 466:75
47. Cabral AM, Trabelsi W, Serra R, Montemor MF, Zheludkevich ML, Ferreira MGS (2006) *Corros Sci* 48:3740
48. Ferreira MGS, Duarte RG, Montemor MF, Simões AMP (2004) *Electrochim Acta* 49:2927
49. Zhao X, Wang J, Wang Y, Kong T, Zhong L, Zhang W (2007) *Electrochem Commun* 9:1394
50. Jorcin JB, Aragon E, Meelatti C, Pèbère N (2006) *Corros Sci* 48:1779
51. Palomino LE, de Castro JFW, Aoki IV, de Melo HG (2003) *J Braz Chem Soc* 14:651